



**Multifunctional human serum albumin modified reduced graphene oxide for targeted photothermal therapy of hepatocellular carcinoma**

Journal:	<i>RSC Advances</i>
Manuscript ID	RA-ART-11-2015-024785.R1
Article Type:	Paper
Date Submitted by the Author:	05-Jan-2016
Complete List of Authors:	Zheng, Aixian; Mengchao hepatobiliary hospital of Fujian Medical University, The liver center of Fujian Province Zhang, Da; Mengchao hepatobiliary hospital of Fujian Medical University, The liver center of Fujian Province Wu, Ming; Mengchao hepatobiliary hospital of Fujian Medical University, The liver center of Fujian Province Yang, HH; Fuzhou University, Liu, Xiaolong; Mengchao hepatobiliary hospital of Fujian Medical University, The liver center of Fujian Province Liu, Jingfeng; Mengchao hepatobiliary hospital of Fujian Medical University, The liver center of Fujian Province
Subject area & keyword:	Carbon nanomaterials < Nanoscience



## Multifunctional human serum albumin modified reduced graphene oxide for targeted photothermal therapy of hepatocellular carcinoma

Aixian Zheng<sup>a,b</sup>, Da Zhang<sup>a,b</sup>, Ming Wu<sup>a,b</sup>, Huanghao Yang<sup>d</sup>, Xiaolong Liu<sup>\*a,b</sup>, and Jingfeng Liu<sup>\*a,b,c</sup>

Received 00th January 20xx,  
Accepted 00th January 20xx

DOI: 10.1039/x0xx00000x

[www.rsc.org/](http://www.rsc.org/)

Hepatocellular carcinoma (HCC) is one of the most common cancers worldwide, which had high malignant degree and poor prognosis. Early diagnosis and treatment of HCC would significantly improve the clinical outcomes. Near infrared (NIR) laser and photo-absorbing agent based photothermal therapy (PTT) is an emerging hyperthermia therapeutic approach, and has been suggested as a minimally invasive and highly efficient therapeutic method. Reduced graphene oxide (rGO) is one of the most typical photothermal agents. Compared with other materials, rGO possesses some advantages, such as simple synthesis, low cost, high photo-stability and large surface area for drug loading. However, rGO exhibits poor dispersibility and difficulty modification by losing the hydrophilic functional groups during reduction process. Thus, the modification processes of rGO are always complicated, time-consuming, and require some expensive polymers. In this paper, Human serum albumin (HSA) was functionalized with indocyanine green (ICG) and lactobionic acid (LA) to prepare the multifunctional human serum albumin (mfHSA), which could be used for the modification of rGO. This approach is simple and high efficient, which not only improves the stability and the biocompatibility of rGO, but also makes them exhibit the enhanced photothermal conversion efficiency and the targeting specificity to HCC cells. The low cytotoxicity and the PTT therapeutic efficacy at both cellular and animal levels indicated that the prepared multifunctional nanomaterials could be expected to serve as a highly effective therapeutic agent for HCC.

### Introduction

Hepatocellular carcinoma (HCC) is one of the most common cancers worldwide, which is also the third leading cause of cancer-related death.<sup>1</sup> Most of the HCC patients were diagnosed at the late stage of the disease, resulting in limited clinical outcomes and poor prognosis. Thus, early diagnosis and treatment of HCC is urgent needed to improve the therapeutic effects and prolong the survival time. Recently, various new imaging agents, drug delivery systems and diagnostic methods have been widely explored.<sup>2</sup> Among them, near infrared (NIR) laser induced photothermal therapy (PTT) has received significant interests in recent years. PTT is an emerging hyperthermia therapeutic approach with the help of photothermal agents that can effectively absorb the near

infrared (NIR) laser and then convert into heat to kill cancer cells.<sup>3</sup> Compare with traditional therapeutic strategies such as chemotherapy and radiotherapy, NIR laser induced PTT has been suggested as a minimally invasive and highly efficient therapeutic method.<sup>4</sup>

Recently, a variety of materials, such as organic fluorescent dyes, carbon nanomaterials,<sup>5</sup> gold nanomaterials,<sup>6</sup> copper sulfide nanoparticles,<sup>7</sup> palladium nanosheets<sup>8</sup> and organic nanoparticles,<sup>9</sup> have been explored as photothermal agents for PTT due to their high absorption in tissue-transparent NIR region (700-900nm), and some of them have entered clinical trials. Among them, Indocyanine green (ICG) is the Federal Drug Administration approved clinical agent for NIR fluorescence imaging.<sup>10</sup> Due to the strong NIR absorption, ICG can be also used for NIR laser induced PTT. However, ICG has some disadvantages such as poor photo-stability, concentration-dependent aggregation and non-specific binding to proteins, which may limit its applications.<sup>11</sup> Reduced graphene oxide (rGO), one of the most typical photothermal nanomaterials, has attracted much attention in recent years. The rGO exhibits strong NIR absorption and high photothermal conversion efficiency, making it can be used as photoacoustic contrast and photothermal agent for the diagnosis and treatment of cancer.<sup>12</sup> Compared with other materials, rGO possesses some advantages, such as simple synthesis, low cost, high photo-stability and large surface area for drug loading. However, the hydrophilic functional groups contained in rGO

<sup>a</sup>The United Innovation of Mengchao Hepatobiliary Technology Key Laboratory of Fujian Province, Mengchao Hepatobiliary Hospital of Fujian Medical University, Fuzhou 350025, P. R. China.

<sup>b</sup>The Liver Center of Fujian Province, Fujian Medical University, Fuzhou 350025, P. R. China.

<sup>c</sup>Liver Disease Center, The First Affiliated Hospital of Fujian Medical University, Fuzhou 350005, P. R. China.

<sup>d</sup>The Key Lab of Analysis and Detection Technology for Food Safety of the MOE, College of Chemistry, Fuzhou University, Fuzhou 350108, P. R. China.

E-mail: [xiaolong.liu@gmail.com](mailto:xiaolong.liu@gmail.com); [drjingfeng@126.com](mailto:drjingfeng@126.com).

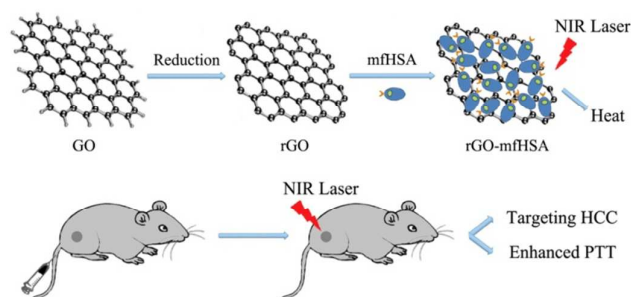
Electronic Supplementary Information (ESI) available: [details of any supplementary information available should be included here]. See

DOI: 10.1039/x0xx00000x

were significantly decreased during reduction from graphene oxide<sup>13</sup> (GO), which may cause poor dispersibility<sup>14</sup> and difficulty modification. For in vivo applications, appropriate surface modification of rGO is necessary to improve the dispersibility and biocompatibility. However, these modification processes are always complicated, time-consuming, and require some expensive polymers.<sup>15</sup> For example, Cai and coworkers used Boc-NH-PEGNH<sub>2</sub> and C<sub>18</sub>PMH to obtain C<sub>18</sub>PMH-PEG<sub>5000</sub>-NH<sub>2</sub> by deprotection of the Boc group with trifluoroacetic acid. After purification, the prepared polymer was then used to modify rGO via hydrophobic interactions between the C18 chains and the rGO surface.

It has been reported that protein can be adsorbed on the surface of rGO through the hydrophobic and  $\pi$ - $\pi$  stacking interactions. Thus, human serum albumin (HSA) could be intended as the stabilizer of rGO, which is a natural protein that presents in all parts of the human body. It is noteworthy that specific targeting of therapeutic agents to cancer cells could improve the therapy efficacy due to the decreased toxicity to normal tissues and the increased local dose at treatment site. Galactose residues are one of the most attractive targeting ligand for HCC due to its high affinity to the asialoglycoprotein receptor (ASGP-R), which is highly expressed on the surface of HCC cells.<sup>16</sup> HSA could be covalently conjugated with lactobionic acid (LA) between the amine groups of the protein and the carboxy groups of LA to introduce the galactose residues for HCC cell targeting. Moreover, ICG can noncovalently attach to HSA,<sup>17</sup> which can be protected by rGO from degradation and thus enhance the photothermal conversion efficiency of rGO.

In this paper, HSA was functionalized with ICG and LA to prepare the multifunctional human serum albumin (mfHSA), which could be used as the stabilizers of rGO to prepare the multifunctional therapeutic agents (scheme 1). This approach is simple and high efficient, which not only improves the stability and the biocompatibility of rGO, but also makes them possess some other excellent features to improve the therapeutic efficacy of PTT, such as the increased photothermal conversion efficiency and the targeting specificity to HCC cells. We will investigate the PTT therapeutic efficacy of prepared multifunctional nanomaterials at both cellular and animal levels.



**Scheme 1** Schematic presentation of mfHSA modified rGO as therapeutic agents for targeted photothermal therapy of Hepatocellular Carcinoma.

## Experimental

### Materials and apparatus

Graphite powder was purchased from Sinopharm Chemical Reagent Co., Ltd; HSA was purchased from Bomei Co. Ltd; LA was purchased from J&K Scientific Ltd; Indocyanine green (ICG) was purchased from Tokyo Chemical Industry Co., Ltd; N-(3-dimethylaminopropyl)-N-ethylcarbodiimide hydrochloride (EDC) and sulfo-N-hydroxysuccinimide (sulfo-NHS) were purchased from Sigma-Aldrich Co.; Cell Counting Kit-8 (CKK-8) was purchased from Dojindo Laboratorie; and Live-Dead Viability/Cytotoxicity Kit (Calcein AM/EthD-1) was purchased from life technologies, Inc. All other reagents were of analytical grade. Ultrapure water (18.2 M $\Omega$ -cm) was obtained from a Millipore water purification system and was used in all experiments.

The absorbance data were all measured by microplate reader (Spectra Max M5, Molecular Devices). The fluorescent spectra were measured by Cary Eclipse fluorescence spectrophotometer (Agilent Technologies, Malaysia). The particle size and the zeta potential were determined by dynamic light scattering (DLS) using the Zetasizer Nano ZS (Malvern Instruments, UK). Atomic force microscopic (AFM) images of GO and rGO were taken using a Nanoscope III multimode atomic force microscope (USA) in tapping mode. Raman spectra of GO and rGO were recorded on a Renishaw inVia laser Raman spectrometer. NIR laser irradiation was performed using a continuous-wave diode NIR laser with a center wavelength of 808 nm (K808D/K09F-8.00W, Beijing Kaipulin Optoelectronic Technology Co., China). Fluorescence imaging of live/dead cells was performed with a confocal laser scanning fluorescence microscope (Zeiss LSM780). The Hematoxylin and eosin (H&E) staining and Immunohistochemical staining of major organs and tumor tissues were observed by Zeiss microscope (Axio Lab.A1).

### Cell culture

The human hepatocellular carcinoma cell line (HepG2) and the human cervical cancer cell line (HeLa) were maintained as a monolayer culture in MEM and RPMI-1640 medium at 37 °C in a humidity atmosphere (5% CO<sub>2</sub>). They were both supplemented with 10% fetal bovine serum (FBS, Atlanta Biologicals, Lawrenceville, GA, USA) and 1% penicillin-streptomycin (Gibco BRL, Grand Island, NY, USA).

### Preparation of GO and rGO

GO was prepared according to a modified Hummers method.<sup>18</sup> In the detail procedure, 1g of graphite powder and 1g NaNO<sub>3</sub> were milled for 20min, and then mixed with 46mL concentrated H<sub>2</sub>SO<sub>4</sub> in glass beaker under ice bath. After slowly added of 6g KMnO<sub>4</sub>, the mixture was put in a water bath at 35°C and stirred for about 2h. Then, 80mL of ultrapure water were added to the above beaker and stirred at 90°C for 35min. After extra addition of 200mL ultrapure water, 6mL 30% H<sub>2</sub>O<sub>2</sub> was slowly added into the mixture. In this process, the color of the mixture turned from brown to yellow. After cooling down to room temperature, the mixture was centrifuged at 10000rpm for 5min (3 times) to remove the

exceeded acid. Then the suspension was centrifuged at 2000rpm for 5min (3 times) to separate the impurities. The supernatant was collected and then continued to centrifuge at 16000 rpm for 20min (3 times). Finally, the sediment was collected and vacuum dried. 20mg of the obtained solid was then dispersed in 20mL ultrapure water by sonication for 4h to obtain the GO solution.

To prepare rGO, the solution was centrifuged at 10000rpm for 10min to isolate the large size of GO. Then, 300 $\mu$ L of ammonia solution was added to the supernatant. After stirred for a moment, the mixture was transferred to 50mL of polytetrafluoroethylene (PTFE) lined stainless-steel autoclave and reacted at 100°C for 3h. After cooling down to room temperature, the mixture was further dialyzed in a dialysis bag (retained molecular weight: 3500Da) for 3 days.

#### Preparation of mfHSA modified rGO (rGO-mfHSA)

ICG was noncovalently conjugated to HSA by simple mixing. Typically, 10mL of 10 $\mu$ M HSA in PBS buffer was mixed with 1mL 600 $\mu$ M ICG and then shaken for 4h at room temperature. To remove the unbound ICG, the mixture was dialyzed in a dialysis bag (retained molecular weight: 3500Da) for 2days.

The mfHSA was prepared by the covalently linking of active LA and HSA-ICG complex. Firstly, 1mL of 5mM LA was reacted with 3mg EDC and 3mg sulfo-NHS for 1h at room temperature. Then, 100 $\mu$ L of the activated LA was reacted with 10mL of the HSA-ICG complex for 24h at room temperature. Finally, the solution was dialyzed in a dialysis bag (retained molecular weight: 3500Da) for 2days to remove the unreacted active LA and other reaction byproducts.

Finally, 4mL of mfHSA solution were mixed with 6mL of 0.6mg mL<sup>-1</sup> rGO solution and then shaken for 12h at room temperature. The obtained rGO-mfHSA was purified by centrifugation at 20000rpm for 30min (twice).

#### Photothermal effect induced by NIR laser

The photothermal effect of the prepared rGO or rGO-mfHSA induced by NIR laser was evaluated by monitoring the temperature change of the corresponding solution with different concentrations (0, 5, 10 and 20 $\mu$ g mL<sup>-1</sup>). Briefly, 1.0 mL of the solution were added to a quartz cuvette and then irradiated by an NIR laser (808nm 2W cm<sup>-2</sup>) for 10min. The temperature change of the solution was monitored by a thermocouple microprobe. Meanwhile, the photothermal effect of water, ICG and mfHSA was evaluated for comparison.

#### In vitro cytotoxicity and photothermal ablation ability

The in vitro cytotoxicity of rGO-mfHSA was evaluated on 3T3 Cells and HepG2 cells using a Cell Counting Kit (CCK-8). The cells were seeded in a 96-well plate and incubated in humidity atmosphere (5% CO<sub>2</sub>) at 37°C for 24h. After washed three times with PBS, the cells were further incubated with different concentrations (0, 20, 40, 60, 80, 100 $\mu$ g mL<sup>-1</sup>) of rGO-mfHSA (at rGO concentration) for 24h or 48h, respectively. After washed three times, the cell survival rates were measured by CCK-8 according to the manufacturer's protocol. The results represent the average of four independent experiments.

CCK-8 was also used to study the photothermal ablation ability of rGO-HSA-LA and rGO-mfHSA against HepG2 cells. Typically,

hepG2 cells were seeded in a 96-well plate at a density of 1  $\times$  10<sup>4</sup> cells per well and incubated at 37°C for 24 h in humidity atmosphere (5% CO<sub>2</sub>). After washed three times with PBS, the cells were incubated with different concentrations (0, 5, 10, 20, 40 $\mu$ g mL<sup>-1</sup>) of rGO-HSA-LA or rGO-mfHSA for 4h. After washed three times with PBS, the cells of each well were irradiated with a NIR laser (808nm, 2W cm<sup>-2</sup>) for 5 min. Then, CCK8 was used to measure the cell survival rate.

To further evaluate the photothermal cytotoxicity of rGO-mfHSA, we used the Live-Dead Viability/Cytotoxicity Kit to stain the cells after laser irradiation. Firstly, HepG2 cells (2  $\times$  10<sup>5</sup>) and HeLa cells (5  $\times$  10<sup>4</sup>) were seeded in a 35mm glass-bottom Petri dish and incubated at 37°C for 24h in humidity atmosphere (5% CO<sub>2</sub>). After washed three times with PBS, the cells were incubated with 20 $\mu$ g mL<sup>-1</sup> rGO-mfHSA for 4h at 37°C. Subsequently, the cells were washed three times with PBS and then irradiated with NIR laser (808nm, 2W cm<sup>-2</sup>) for 5min. Finally, the cells were stained with 2.0 $\mu$ M calcein AM and 4.0 $\mu$ M EthD-1 for the visualization of live and dead cells.

#### Tumor xenograft and in vivo photothermal cancer therapy

Male BALB/c-nude mice (5-6 weeks old) were purchased from China Wushi, Inc. All animal procedures were performed according to the national and institutional guidelines and approved by the Animal Ethics Committee of Fujian Medical University (SYXK (fujian) 2012-0001). The tumors were generated by subcutaneous injection of HepG2 cells (10<sup>7</sup>) in sterilized PBS onto the back of the mice. When the tumor size reached 150-200mm<sup>3</sup>, the mice were divided into three groups and each group has six mice. Two groups were tail-vein injected with 200 $\mu$ L of 1mg mL<sup>-1</sup> rGO-HSA-ICG and rGO-mfHSA (at rGO concentration), respectively. The other group were tail-vein injected with 200 $\mu$ L PBS and used as control.

The NIR laser irradiation at tumor sites was performed after 18h of tail vein injection, and the temperature changes can be observed by the thermo-graphic images. To examine the histological changes of the treated tumor tissues, one mouse in each group was sacrificed and the tumors were collected after 24h. The treated tumor tissues were stained with Hematoxylin and eosin (H&E) for histopathology evaluation and Ki67 antibody for immunohistochemical analysis. The effects of photothermal treatment of nanomaterials were evaluated by monitoring the changes of tumor volume and body weight of the mice in each group.

#### In vivo toxicity of rGO-mfHSA

Male ICR mice (4-5 weeks old) were obtained from the Center for Animal Experiment of Fujian Medical University. To evaluate the in vivo toxicity of rGO-mfHSA, each four healthy mice were tail-vein injected with 200 $\mu$ L of 1mg mL<sup>-1</sup> rGO-mfHSA for 1, 3, and 7days. Other four mice were tail-vein injected with 200 $\mu$ L PBS and used as control. Blood specimen of each mouse was collected by orbital blood collection. After standing for one hour, the blood samples were centrifuged at 3000rpm for 10min to obtain the serum, which can be used for biochemical examinations. The biochemical parameters including alanine aminotransferase (ALT), aspartate transaminase (AST), blood urea nitrogen (BUN) and creatinine

## ARTICLE

(Cr) were measured according to the manufacturer's protocol. Meanwhile, to perform the histopathological analysis, the major organs of the mouse in each group were collected and then fixed in 4% neutral buffered formalin. After processed, the corresponding tissues (heart, liver, spleen, lung and kidney) were stained with H&E for histopathology evaluation.

## Results and discussion

### Preparation and characterization of mfHSA modified rGO

GO was prepared according to a modified Hummers method. Fig. 2A shows the AFM image of GO by simultaneously collecting the height and phase data. The average thickness of GO was about 1nm, implying that they are single-layered structure. Meanwhile, the average size of GO was about 200nm. When reduced by ammonia, GO can be further converted into rGO. And the color of the solution was changed from yellow to black, resulting in increased optical absorption in NIR region (Fig. 1A). This result is consistent with previous reports<sup>12</sup>. The structural changes from GO to rGO can be also characterized by Raman spectra. As respected, GO has two prominent Raman bands, D band at around 1348  $\text{cm}^{-1}$  and G band at around 1594  $\text{cm}^{-1}$ , respectively. After reduction, the obtained rGO also has the D band and the G band but increasing the D/G intensity ratio compared to that of GO (Fig. 1B), indicating the successful conversion of GO to rGO.

HSA can be adsorbed on the surface of GO through the hydrophobic and  $\pi$ - $\pi$  stacking interactions as well as maintain the stability (Fig. S1 in ESI). Thus, we consider the use of mfHSA to modify rGO. To obtain the mfHSA, HSA was noncovalently attached with ICG and then further covalently conjugated with LA between the carboxy groups of LA and the amine groups of the protein molecule. After conjugated with LA, the zeta potential of the protein was changed from -12.3 to -17.2. On the other hand, the successful attaching of ICG to HSA was easily evidenced by the presence of characteristic absorption peaks of ICG and the slight red-shift phenomenon (Fig. S2 in ESI). Then the HSA-ICG complex was further conjugated with LA to obtain the mfHSA. The presence of galactose residues on mfHSA can be determined by the phenol-vitriol method.

The successful preparation of rGO-mfHSA can be confirmed by the appearing of NIR absorption peak (Fig. 1C) and the significantly quenched fluorescence of the complexes (Fig. 1D). Since ICG in the mfHSA exhibited high NIR absorption and the fluorescence can be quenched when close to rGO surface. It was estimated that 0.334 mmol/g of ICG in mfHSA was adsorbed onto the rGO surface, which was calculated by the standard curve (Fig. S3 in ESI) and subtracting the amount in the supernatant. As shown in Fig. 2B, after the reaction of mfHSA with rGO, the average thickness of the complex was increased to about 4nm. Meanwhile, the morphology and the zeta potential values of the nanomaterials were significantly changed after modification (Fig. S4 in ESI). These results can further confirm the successful functionalization of rGO.

## RSC Advances

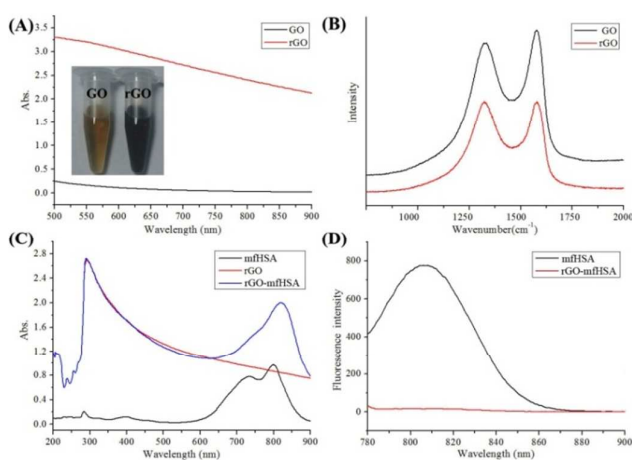


**Fig. 1** (A) Absorption spectra and photograph of 0.6mg mL<sup>-1</sup> GO and rGO; (B) Raman spectra of GO and rGO; (C) absorption spectra of rGO, mfHSA and rGO-mfHSA; (D) fluorescence spectra of mfHSA and rGO-mfHSA.

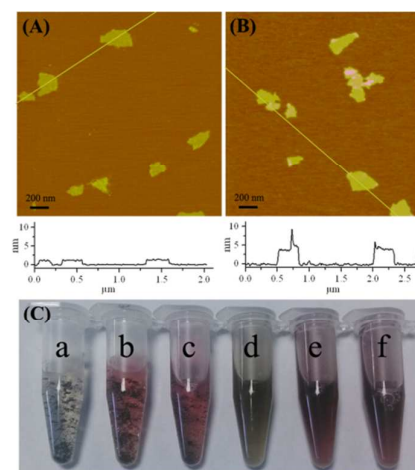


**Fig. 2** (A) AFM image of rGO and rGO-mfHSA deposited on mica substrates by simultaneously collecting the height and phase data; (B) the dispersibility of rGO (a-c) and rGO-mfHSA (d-f) in PBS, MEM Medium and MEM Medium containing 10% serum.

Furthermore, the prepared rGO-mfHSA exhibited high stability in PBS buffer and other biological mediums, while rGO was aggregated in these mediums due to  $\pi$ - $\pi$  stacking interactions (Fig. 2C). The results of *in vitro* release behaviour and confocal microscopy images (Fig. S5 in ESI) all indicated that mfHSA could be stable on the surface of rGO. Apart from the stabilizing effect, the protein layer on rGO surface could also increase their biocompatibility due to the intrinsic nature of HSA itself.

### Temperature elevation induced by NIR laser irradiation

The high NIR absorption of rGO-mfHSA suggested that it would be a good photo-absorbing agent for PTT. The photothermal effect of rGO-mfHSA was investigated by monitoring the temperature change of the solution induced by NIR laser irradiation. As shown in Fig. 3A, after exposure to NIR laser irradiation for 10 min, the temperature of the solution with 5,

10, and  $20\mu\text{g mL}^{-1}$  rGO-mfHSA (at rGO concentration) increased by 18.4, 25.9, and  $32.2^\circ\text{C}$ , respectively. The temperature of the solution can increase up to  $59.3^\circ\text{C}$  when the concentration of rGO-mfHSA up to  $20\mu\text{g mL}^{-1}$ , which is sufficient to kill cancer cells. While, the temperature of rGO solution with same concentrations increased much slower when exposed to laser irradiation (Fig. 3B). Meanwhile, temperature elevation of equivalent amount of the materials (rGO-mfHSA, rGO, mfHSA and ICG) induced by NIR laser irradiation was also investigated. As shown in Fig. 3C, rGO-mfHSA showed the best photothermal conversion capability, which may due to the combined effect of ICG and rGO. These results suggest that the prepared rGO-mfHSA could be used as an efficient photo-absorbing agent for PTT.

The photothermal stability of nanomaterials is also important in NIR laser induced PTT. To investigate the photothermal stability of rGO-mfHSA, the solution was subjected to three rounds of on/off laser irradiation. As shown in Fig. 3D, rGO-mfHSA showed excellent photothermal stability during repeated laser irradiation, while the photothermal effect of ICG was obviously reduced during the same process. This is because that ICG is easily degraded by laser irradiation, while rGO can protect it from being degraded.

#### In vitro cytotoxicity of rGO-mfHSA

Nontoxicity or low toxicity of nanomaterials is another important aspect for PTT. The CCK-8 was used to investigate the in vitro cytotoxicity of rGO-mfHSA, and the HepG2 cells and 3T3 normal cells were used as cell models. As shown in Fig. 4, the viability of both cells remained more than 90% even with the incubation of  $100\mu\text{g mL}^{-1}$  rGO-mfHSA (at rGO concentration) for 24h or 48h. Thus, the prepared multifunctional nanomaterials have good biocompatibility and low cytotoxicity to both HepG2 cells (A) and 3T3 cells (B) without laser irradiation.

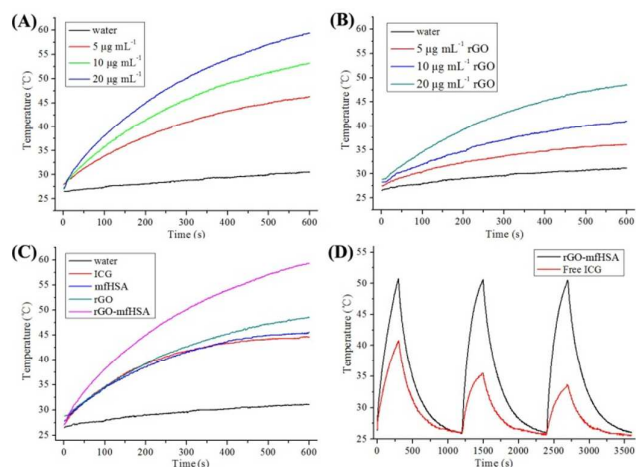


**Fig. 3** Temperature changes of different concentrations of rGO-mfHSA (A) and rGO (B) after exposure to NIR laser ( $808\text{nm}$ ,  $2\text{W cm}^{-2}$ ) for 10min, water was used as a control; (C) Temperature changes of rGO ( $20\mu\text{g mL}^{-1}$ ) and corresponding concentrations of free ICG, mfHSA and rGO-mfHSA after exposure to NIR laser for 10 min; (D) Temperature changes of rGO-mfHSA and free ICG solution subjected to three rounds of on/off laser irradiation.

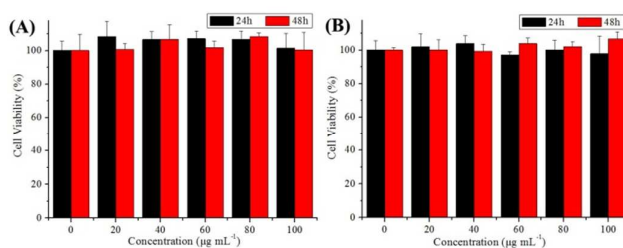


**Fig. 4** Cell viability of 3T3 cells (A) and HepG2 (B) cells treated with different concentrations of rGO-mfHSA for 24h or 48h (without laser irradiation).

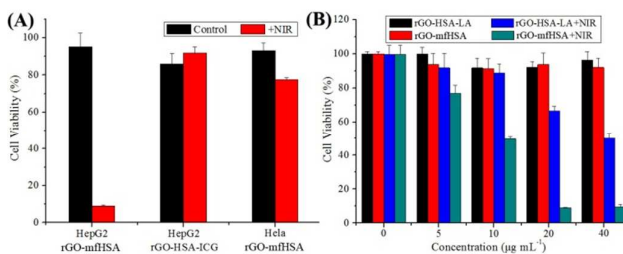


**Fig. 5** (A) Cell viability of HepG2 cells treated with  $20\mu\text{g mL}^{-1}$  rGO-mfHSA and rGO-HSA-ICG, or the HeLa cells incubated with  $20\mu\text{g mL}^{-1}$  rGO-mfHSA; (B) Cell viability of HepG2 cells treated with different concentrations of rGO-HSA-LA and rGO-mfHSA. The cells were irradiated with NIR laser ( $808\text{nm}$ ,  $2\text{W cm}^{-2}$ ) for 5 min or without laser irradiation as control.

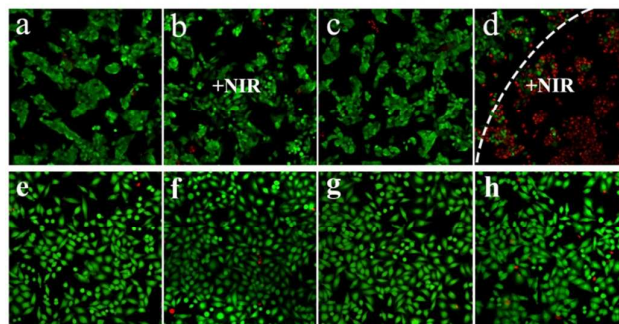


**Fig. 6** Confocal micrographs of hepG2 cells (a-d) and HeLa cells (e-h) stained with calcein AM (green, live) and EthD-1 (red, dead). (a, e) untreated cells; (b, f) treated with  $20\mu\text{g mL}^{-1}$  rGO-mfHSA; (c, g) NIR laser irradiation for 5min; (d, h) treated with  $20\mu\text{g mL}^{-1}$  rGO-mfHSA combined with NIR laser irradiation for 5min.

#### In vitro photothermal ablation ability

The photothermal ablation ability of rGO-mfHSA was analyzed by using CCK-8 and Live-Dead Viability/Cytotoxicity Kit. To improve the delivery efficiency into HCC cells, the multifunctional nanomaterials have been modified with LA. The generated galactose residues can be used as the targeting ligand for HCC due to its high binding affinity to ASGP-R, which is highly expressed on the surface of HCC cells.

As shown in Fig. 5A, HepG2 cells were incubated with rGO-HSA-ICG or rGO-mfHSA at the same rGO concentration ( $20\mu\text{g mL}^{-1}$ ) for 4h and then exposure to laser irradiation for 5min.

We can find that the viability of HepG2 cells incubated with rGO-mfHSA decreased by about 90%, while the HepG2 cells incubated with rGO-HSA-ICG still maintained high viability. This result indicated that the modification of LA can really improve the delivery efficiency into HCC cells. On the other hand, when HeLa cells were used instead of HepG2 cells to incubate with rGO-mfHSA, the cell viability remained more than 75%, which is much higher than that of HepG2 cells. This is because that the amount of ASGP-R on the surface of HeLa cells is much lower than that of HepG2 cells, which is the target of galactose residues. These results indicated that the prepared multifunctional nanomaterials can be used to selectively target and effectively kill HCC cells.

Moreover, rGO-mfHSA exhibited dose-dependent PTT effect when exposure to laser irradiation. As shown in Fig. 5B, the viability of HepG2 cells decreased by about 90% when the concentration of rGO-mfHSA up to  $20\mu\text{g mL}^{-1}$  (at rGO concentration). While, the viability of the cells just decreased to 49.8% even if they were incubated with double concentration of rGO-HSA-LA. This result indicated that the modification of rGO with mfHSA not only introduce the capability of targeting to HCC cells, but also enhance the PTT efficacy due to the combined effect of ICG and rGO.

To further evaluate the targeted therapeutic effect of rGO-mfHSA, the treated HeLa and HepG2 cells were stained with Calcein AM and EthD-1 to visualize the live and dead cells, which could exhibit green and red fluorescence, respectively. As shown in Fig. 6, the HepG2 cells showed almost green fluorescence when treated with  $20\mu\text{g mL}^{-1}$  rGO-mfHSA alone or exposed to NIR laser irradiation alone, indicating low toxicity of prepared nanomaterials or NIR laser irradiation alone. However, red fluorescence region of dead cells was observed when the cells were simultaneously treated with rGO-mfHSA and laser irradiation. This phenomenon clearly demonstrated that the prepared rGO-mfHSA had excellent therapeutic effect against HCC cells. When using HeLa cells as targets, the vast majority of green fluorescence indicated that most of the cells were viable even if they were simultaneously treated with rGO-mfHSA and laser irradiation. These results once again indicated that the prepared multifunctional nanomaterials can specifically target to HCC cells and effectively kill them with the help of NIR laser.

#### Photothermal treatment of rGO-mfHSA in vivo

The targeted photothermal therapy of the prepared multifunctional nanomaterials was further performed in tumor-bearing nude mice. Two groups of the mice were tail-vein injected with  $200\mu\text{L}$  of  $1\text{mg mL}^{-1}$  rGO-HSA-ICG and rGO-mfHSA (at rGO concentration), respectively. The other group of the mice were tail-vein injected with  $200\mu\text{L}$  PBS and used as control. After 18h of tail vein injection, the tumor sites of the mice were exposed to NIR laser, and the temperature changes of which can be observed by the thermo-graphic images. As shown in Fig. 7A and 7B, after 10min laser irradiation, the tumor temperature of the rGO-mfHSA treated mice can increase to  $50.5^\circ\text{C}$ , which is high enough to kill cancer cells. While, the tumor temperature of the rGO-HSA-ICG treated

mice can only increase to  $45.5^\circ\text{C}$ , which indicating that the modification of LA can improve the photothermal effect due to the enhanced accumulation of nanomaterials in tumor sites by specifically targeting to HCC cells. This result was further demonstrated by histopathological analysis and immunohistochemical analysis. The related tumor tissues have been collected and stained with H&E for histopathology evaluation. As shown in Fig. 7C, the tumor tissue of PBS treated mice had no necrosis or obvious apoptosis and the tumor cells have normal morphology, indicating that the laser irradiation under experimental condition is not enough to kill cancer cells. Compare with them, the tumor tissue of rGO-HSA-ICG treated mice showed a certain degree of cellular damage at tumor site. And the rGO-mfHSA treated mice showed significant cell destruction at tumor site, including cells shrinkage, nucleus damage and the loss of contact. The treated tumor tissues of each group were also stained with Ki67 antibody for immunohistochemical analysis, since Ki67 can be used to reflect cell proliferation status.<sup>19</sup> As shown in Fig. 7D, the Ki67 was significantly expressed at the tumor site of control mouse, indicated by the large number of the brown granules in the cell nucleus. The expression of Ki67 was slightly decreased in the rGO-HSA-ICG treated group, and it was greatly decreased in the rGO-mfHSA treated group. These results indicated that the prepared multifunctional nanomaterials could be used for PTT in vivo by causing cellular destruction and significant decrease of cell proliferation. Furthermore, the modification of LA can improve the therapeutic efficacy of PTT.

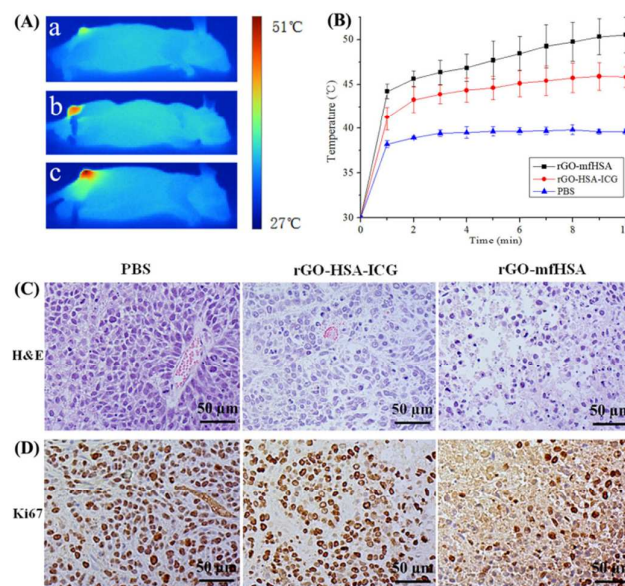


**Fig. 7** (A) Thermo-graphic images of tumor bearing nude mice that tail-vein injected with  $200\mu\text{L}$  PBS (a),  $200\mu\text{g}$  rGO-HSA-ICG (b) and rGO-mfHSA (c) for 18h and then exposed to laser irradiation (808 nm, 1 W) for 10min. (B) The corresponding temperature change of tumor sites for 10min; (C) H&E staining and (D) immunohistochemical staining of the tumor tissues after treatment for 24 h.

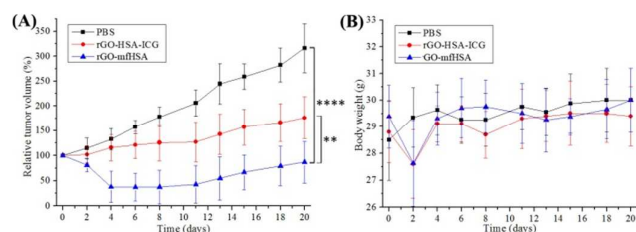


**Fig. 8** (A) Relative tumor volumes (%) of the mice after different treatments as indicated; (B) the body weights of the treated mice in different groups. P values were calculated using the nonpaired, two-tailed Student's t test (\*\* $P < 0.01$ , \*\*\*\* $P < 0.0001$ ). The data represent the average of five independent experiments ( $n = 5$ ).

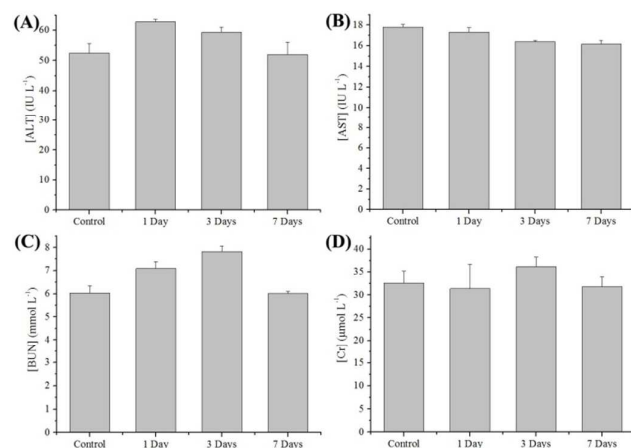


**Fig. 9** Serum biochemical examination of rGO-mfHSA treated mice: (A) alanine aminotransferase (ALT); (B) aspartate transaminase (AST); (C) blood urea nitrogen (BUN); (D) creatinine (Cr). The data represent the average of four independent experiments ( $n = 4$ ).

The therapeutic efficacy of PTT was further investigated by monitoring the change of relative tumor volumes of treated mice for 20 days. As shown in Fig. 8A, the tumor volume of PBS treated mice increased rapidly, indicating that laser irradiation alone had no significant effect on tumor growth. However, the rGO-HSA-ICG and rGO-mfHSA treated groups showed obvious inhibition of tumor growth or even tumor shrinkage, indicating the photothermal therapeutic efficacy of nanomaterials. It is noteworthy that the rGO-mfHSA treated group showed higher therapeutic efficiency than that of rGO-HSA-ICG treated group, which should be due to enhanced accumulation through the specific targeting ability to tumor cells of the modified LA. High toxicity or side effects of nanomaterials usually cause the body weight loss, so the body weight of the mice was also measured after PTT treatment. As shown in Fig. 8B, the mice in each group had no obvious weight loss, indicating that the used therapeutic approach had no significant toxicity or side effects. Therefore, the prepared multifunctional nanomaterials can be expected to serve as a highly effective therapeutic agent for HCC.

#### In vivo toxicity of rGO-mfHSA

In vivo toxicity of the prepared nanomaterials is of great concern before clinical applications. In order to investigate the potential in vivo toxicity, each four healthy ICR mice were tail-

vein injected with 200  $\mu\text{L}$  of 1  $\text{mg mL}^{-1}$  rGO-mfHSA (at rGO concentration) for 1, 3, and 7 days. Other four mice were tail-vein injected with 200  $\mu\text{L}$  PBS and used as control. Then the mice were sacrificed for serum biochemical examination and histopathological analysis. Serum sample of each mouse was collected and used for the detection of biochemical parameters, including two liver function index (ALT and AST) and two kidney function index (BUN and Cr).<sup>20</sup> As shown in Fig. 9, all the values of the measured parameters are within normal ranges and are close to those in control group. This result suggested that the injection of rGO-mfHSA would not cause hepatic and kidney damage. In addition, the major organs (heart, liver, spleen, lung and kidney) of the mice were isolated and stained with H&E for histopathological analysis. As shown in Fig. S6 in ESI, the major organs of the mice had no signs of inflammation or deformities after treated with rGO-mfHSA, and the staining images of which are similar to those in control group. These results indicated that the prepared multifunctional nanomaterials show little or no in vivo toxicity under the experimental conditions.

#### Conclusions

In summary, HSA can be functionalized with ICG and LA, and then used as the stabilizers of rGO. This approach is simple and high efficient, which not only improves the stability of rGO, but also increases the biocompatibility due to the intrinsic nature of HSA itself. Furthermore, the prepared rGO-mfHSA exhibited increased photothermal conversion efficiency due to the combined effect of ICG and rGO. And the generated galactose residues can be used as the targeting ligand for HCC due to its high binding affinity to ASGP-R that is highly expressed on the surface of HCC cells. These multifunctional nanomaterials can specifically target to HCC cells and effectively kill them with the help of NIR laser, which can be further used for PTT in vivo by causing cellular destruction and significant decrease of cell proliferation. The results of serum biochemical examination and histopathological analysis also indicated that these nanomaterials show little or no in vivo toxicity. Thus, these prepared multifunctional nanomaterials could be expected to serve as a highly effective therapeutic agent for HCC.

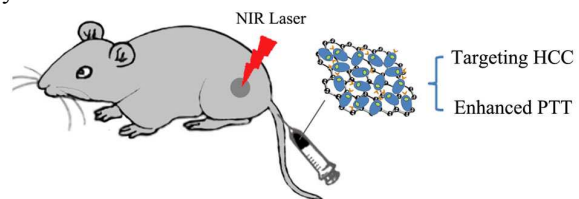
#### Acknowledgements

This work is supported by the key clinical specialty discipline construction program of Fujian, PRC; the Science and Technology Infrastructure Construction Program of Fujian Province (Grant No. 2014Y2005); the specialized Science and Technology Key Project of Fujian Province (Grant No. 2013Y20002-3); the National Natural Science Foundation of China (Grant No. 61575044); the Scientific Foundation of Fuzhou Health Department (Grant Nos. 2015-S-wq9, 2014-S-w18 and 2014-S-w25); the scientific innovation project of Fujian provincial Health and Family Planning Commission (Grant No. 2014-CX-32).

## Notes and references

- 1 Y. H. Tang, T. F. Wen and X. Chen, *Hepato-Gastroenterology*, 2013, **60**, 2019-2025; P. Ferenci, M. Fried, D. Labrecque, J. Bruix, M. Sherman, G. Lau, F. Carillo, J. Krabshuis and A. Le Mair, *J. Gastrointest. J. Gastrointest. Liver Dis.*, 2010, **19**, 311-317; Q. Lai, F. Nudo, G. Mennini, G. Spoletini, V. Morabito, S. G. Levi, F. Melandro, N. Guglielmo, P. B. Berloco, and M. Rossi, *Hepato-Gastroenterology*, 2013, **60**, 2039-2041; J. M. Llovet, J. Fuster, J. Bruix, *Liver Transpl.*, 2004, **10**, 115-120.
- 2 Z. Li, Y. Zeng, D. Zhang, M. Wu, L. Wu, A. Huang, H. Yang, X. Liu and J. Liu, *J. Mater. Chem. B*, 2014, **2**, 3686-3696; P. C. de Souza, A. Ranjan and R. A. Towner, *Nanomedicine*, 2015, **10**, 1515-1534; D. Rand, V. Ortiz, Y. Liu, Z. Derdak, J. R. Wands, M. Taticek and C. Rose-Petruck, *Nano letters*, 2011, **11**, 2678-2683; S. B. Hartono, W. Gu, F. Kleitz, J. Liu, L. He, A. P. J. Middelberg, C. Yu, G. Q. Lu and S. Z. Qiao, *ACS Nano*, 2012, **6**, 2104-2117; J. Liu, B. Wang, S. B. Hartono, T. Liu, P. Kantharidis, A. P. J. Middelberg, G. Q. Lu, L. He and S. Z. Qiao, *Biomaterials*, 2012, **33**, 970-978; Y. Yang, X. Song, Y. Yao, H. Wu, J. Liu, Y. Zhao, M. Tan and Q. Yang, *J. Mater. Chem. B*, 2015, **3**, 4671-4678; L. Li, W. Gu, J. Liu, S. Yan and Z. P. Xu, *Nano Res*, 2015, **8**, 682-694; Y. Chen, D. Ye, M. Wu, H. Chen, L. Zhang, J. Shi and L. Wang, *Adv. Mater.*, 2014, **26**, 7019-7026.
- 3 R. Bardhan, S. Lal, A. Joshi and N. J. Halas, *Acc. Chem. Res.*, 2011, **44**, 936-946; M. P. Melancon, M. Zhou and C. Li, *Acc. Chem. Res.*, 2011, **44**, 947-956.
- 4 Z. Zha, X. Yue, Q. Ren and Z. Dai, *Adv. Mater.*, 2013, **25**, 777-782.
- 5 G. Hong, S. Diao, A. L. Antaris and H. Dai, *Chem. Rev.*, 2015; J. R. Whitney, S. Sarkar, J. Zhang, T. Do, T. Young, M. K. Manson, T. A. Campbell, A. A. Poretzky, C. M. Rouleau and K. L. More, *Lasers Surg. Med.*, 2011, **43**, 43-51; Y. Chen, C. Tan, H. Zhang and L. Wang, *Chem. Soc. Rev.*, 2015, **44**, 2681-2701; Y. Chen, P. Xu, Z. Shu, M. Wu, L. Wang, S. Zhang, Y. Zheng, H. Chen, J. Wang, Y. Li and J. Shi, *Adv. Funct. Mater.*, 2014, **24**, 4386-4396.
- 6 Z. Zhang, L. Wang, J. Wang, X. Jiang, X. Li, Z. Hu, Y. Ji, X. Wu and C. Chen, *Adv. Mater.*, 2012, **24**, 1418-1423; S. Wang, Z. Teng, P. Huang, D. Liu, Y. Liu, Y. Tian, J. Sun, Y. Li, H. Ju, X. Chen and G. Lu, *Small*, 2015, **11**, 1801-1810; Z. Zhang, C. Liu, J. Bai, C. Wu, Y. Xiao, Y. Li, J. Zheng, R. Yang and W. Tan, *ACS applied materials & interfaces*, 2015, **7**, 6211-6219.
- 7 Q. Tian, M. Tang, Y. Sun, R. Zou, Z. Chen, M. Zhu, S. Yang, J. Wang, J. Wang and J. Hu, *Adv. Mater.*, 2011, **23**, 3542-3547; L. Wu, M. Wu, Y. Zeng, D. Zhang, A. Zheng, X. Liu and J. Liu, *Nanotechnology*, 2015, **26**, 025102.
- 8 W. Fang, S. Tang, P. Liu, X. Fang, J. Gong, N. Zheng, *Small*, 2012, **8**, 3816-3822.
- 9 J. Zhou, Z. Lu, X. Zhu, X. Wang, Y. Liao, Z. Ma and F. Li, *Biomaterials*, 2013, **34**, 9584-9592; K. Ke, L. Lin, H. Liang, X. Chen, C. Han, J. Li and H. H. Yang, *Chem. Commun.*, 2015, **51**, 6800-6803; L. S. Lin, Z. X. Cong, J. B. Cao, K. M. Ke, Q. L. Peng, J. Gao, H. H. Yang, G. Liu and X. Chen, *ACS nano*, 2014, **8**, 3876-3883.
- 10 V. L. Dzurinko, A. S. Gurwood and J. R. Price, *Optometry-Journal of the American Optometric Association*, 2004, **75**, 743-755; B. E. Schaafsma, J. S. Mieog, M. Hutteman, J. R. van der Vorst, P. J. Kuppen, C. W. Lowik, J. V. Frangioni, C. J. van de Velde and A. L. Vahrmeijer, *J. Surg. Oncol.*, 2011, **104**, 323-332.
- 11 V. Saxena, M. Sadoqi and J. Shao, *J. Pharm. Sci.*, 2003, **92**, 2090-2097.
- 12 K. Yang, L. Feng, X. Shi and Z. Liu, *Chem. Soc. Rev.*, 2013, **42**, 530-547; K. Yang, S. Zhang, G. Zhang, X. Sun, S. T. Lee and Z. Liu, *Nano letters*, 2010, **10**, 3318-3323; Y. W. Wang, Y. Y. Fu, L. J. Wu, J. Li, H. H. Yang and G. N. Chen, *J. Mater. Chem. B*, 2013, **1**, 2496-2501; Z. Sheng, L. Song, J. Zheng, D. Hu, M. He, M. Zheng, G. Gao, P. Gong, P. Zhang, Y. Ma and L. Cai, *Biomaterials*, 2013, **34**, 5236-5243; J. T. Robinson, S. M. Tabakman, Y. Liang, H. Wang, H. S. Casalongue, D. Vinh and H. Dai, *J. Am. Chem. Soc.*, 2011, **133**, 6825-6831; Y. Yang, A. M. Asiri, Z. Tang, D. Du and Y. Lin, *Materials today*, 2013, **16**, 365-373.
- 13 C. H. Lu, H. H. Yang, C. L. Zhu, X. Chen and G. N. Chen, *Angew. Chem. Int. Ed.*, 2009, **48**, 4785-4787; M. Zhang, B. C. Yin, W. Tan, and B. C. Ye, *Biosens Bioelectron*, 2011, **26**, 3260-3265; X. Sun, Z. Liu, K. Welsher, J. T. Robinson, A. Goodwin, S. Zaric and H. Dai, *Nano research*, 2008, **1**, 203-212; K. Yang, L. Feng, X. Shi and Z. Liu, *Chem. Soc. Rev.*, 2013, **42**, 530-547; B. Tian, C. Wang, S. Zhang, L. Feng and Z. Liu, *ACS nano*, 2011, **5**, 7000-7009.
- 14 T. Kuila, S. Bose, A. K. Mishra, P. Khanra, N. H. Kim and J. H. Lee, *Prog Mater Sci*, 2012, **57**, 1061-1105.
- 15 S. Shi, K. Yang, H. Hong, H. F. Valdovinos, T. R. Nayak, Y. Zhang, C. P. Theuer, T. E. Barnhart, Z. Liu and W. Cai, *Biomaterials*, 2013, **34**, 3002-3009; H. Kim and W. J. Kim, *Small*, 2014, **10**, 117-126.
- 16 M. Zhang, X. Zhou, B. Wang, B. C. Yung, L. J. Lee, K. Ghoshal and R. J. Lee, *J. Controlled Release*, 2013, **168**, 251-261; R. Kumar, W. S. Shin, K. Sunwoo, W. Y. Kim, S. Koo, S. Bhuniya and J. S. Kim, *Chem. Soc. Rev.*, 2015; Y. Zeng, D. Zhang, M. Wu, Y. Liu, X. Zhang, L. Li, Z. Li, X. Han, X. Wei and X. Liu, *ACS Appl. Mater. Interfaces*, 2014, **6**, 14266-14277.
- 17 A. Topete, M. Alatorre-Meda, P. Iglesias, E. M. Villar-Alvarez, S. Barbosa, J. A. Costoya, P. Taboada and V. Mosquera, *ACS nano*, 2014, **8**, 2725-2738; R. Bardhan, N. K. Grady, J. R. Cole, A. Joshi and N. J. Halas, *ACS nano*, 2009, **3**, 744-752.
- 18 C. H. Lu, H. H. Yang, C. L. Zhu, X. Chen and G. N. Chen, *Angew. Chem. Int. Ed.*, 2009, **48**, 4785-4787; J. L. Chen, X. P. Yan, K. Meng and S. F. Wang, *Anal. Chem.*, 2011, **83**, 8787-8793.
- 19 A. F. Bagley, S. Hill, G. S. Rogers and S. N. Bhatia, *ACS nano*, 2013, **7**, 8089-8097; H. J. Kwon, Y. Byeon, H. N. Jeon, S. H. Cho, H. D. Han and B. C. Shin, *J. Control Release*, 2015, **216**, 132-139.
- 20 S. Su, Y. Tian, Y. Li, Y. Ding, T. Ji, M. Wu, Y. Wu and G. Nie, *ACS nano*, 2015, **9**, 1367-1378; Z. Zhou, J. Wang, W. Liu, C. Yu, B. Kong, Y. Sun, H. Yang, S. Yang and W. Wang, *Nanoscale*, 2014, **6**, 12591-12600.

Table of contents entry



The multifunctional human serum albumin modified reduced graphene oxide can specifically target to HCC cells and effectively kill them with the help of NIR laser.